Structure and polarization in epitaxial ferroelectric $PbZr_{0.52}Ti_{0.48}O_3/YBa_2Cu_3O_{7-x}/Nd:YAlO_3$ thin films

A. M. Grishin,[a] M. Yamazato, Y. Yamagata, and K. Ebihara
Department of Electrical and Computer Engineering, Kumamoto University, Kumamoto 860, Japan

(Received 2 September 1997; accepted for publication 5 December 1997)

We fabricate epitaxial $PbZr_{0.52}Ti_{0.48}O_3/YBa_2Cu_3O_{7-x}$ submicron film ferroelectric/superconductor heterostructures on the single-crystal $YAlO_3+1\%Nd_2O_3$ substrate by the pulsed laser deposition technique. Frequency independent low loss tan $\delta=0.04$ and dielectric constant of 950, high electric resistivity ρ (150 kV/cm)$=6\times10^{11}\Omega$ cm, remnant polarization of 32 μC/cm^2, no visible fatigue after 10^7 short bipolar pulses switching indicate excellent electrical performance of the new capacitor structure. The slight crystallite polar axis misalignment and depolarizing effect were found to be responsible for the shape of the apparent polarization loop. The only fitting parameter depolarizing coefficient $N=2.37\times10^{-4}$ gives the best fit between theory and experimental data and corresponds to *prolate ellipsoidal* shaped crystallites with the length-to-diameter ratio of 140. © *1998 American Institute of Physics.* [S0003-6951(98)03305-1]

In recent years, lead-based ferroelectric thin films such as $PbTiO_3$, Pb(Zr, Ti)O_3 (PZT), and (Pb, La)(Zr, Ti)O_3 have gained much attention as attractive materials for the capacitors in dynamic random-access memories (DRAMs), in ferroelectric random access memories (FERAMs), and the gate dielectric candidates in metal/ferroelectric/semiconductor field-effect transistors (MFSFETs).[1,2] Recent observation of electron emission from cool low voltage PZT thin film cathodes[3] has opened new perspectives in the application of ferroelectric films to emissive plasma display panels.

The operation of all of these devices is based on the remnant polarization of the ferroelectric capacitor. A reversal of polarization releases the switching charge used as a readout signal in a FERAM or as a source of energetic electrons in pulsed high brightness electron sources. High and endurable remnant polarization, great fatigue resistance, acceptable polarization retention as well as low leakage current are commonly desirable characteristics for the vast number of ferroelectric films applications. However, an incorporation of ferroelectric capacitors in actual semiconductor circuits demands specific properties of these functional materials.

In a destructive readout (DRO) memory devices the ratio between the switching part of polarization and ''dielectric'' (nonremnant) polarization is desired to be as high as possible to decrease backswitching of the ferroelectric material. It arises due to the voltage of opposite polarity across the reference capacitor.[4] On the contrary, to increase the signal-to-noise ratio in nondestructive readout (NDRO) memories ferroelectrics with the incremental polarizability at zero bias field as high as possible are needed. Generally, material processing technology should be able to ''engineer'' ferroelectric with the required shape of the polarization loop and dynamics of polarization switching. Although a tremendous breakthrough has been achieved in the complex oxide film processing technique,[5,6] it is still too less known how the structural parameters, composition variable and strain control statics and dynamics of the polarization in thin ferroelectric films.

In this work epitaxial $PbZr_{0.52}Ti_{0.48}O_3/YBa_2Cu_3O_{7-x}/Nd:YAlO_3$ heterostructures have been prepared to fabricate capacitors with highly reproducible and endurable characteristics. The correlation between the structural and ferroelectric characteristics has been revealed. The hysteresis loop calculated in the mean-field approximation accounts for two effects caused by polycrystallinity: depolarizing electric fields of small crystallites and polar axis misalignment, and nicely fits the experimental $P-E$ curve.

$PbZr_{0.52}Ti_{0.48}O_3$(400 nm)/$YBa_2Cu_3O_{7-x}$(200 nm) thin film heterostructures have been prepared *in situ* by pulsed laser deposition technique on the single-crystal *neodymium doped yttrium monoaluminate* substrate of the following composition [$YAlO_3+1\%Nd_2O_3$], hereafter referred to as Nd:$YAlO_3$. This is a perovskite-like crystal of orthorhombic symmetry with space group $D_{2h}^{16}(Pbnm)$ and lattice constants $a=0.5179$ nm, $b=0.5328$ nm, $c=0.7369$ nm.[7,8] The main advantage of the proposed single crystal is a lack of twinning and structural phase transitions in the processing temperature window (see below) and high crystallographic anisotropy which yields the heteroepitaxial growth of complex oxide multilayers. Among additional strengths of this material, the substrate is possessed of the low loss tan δ(10 MHz, 300 K)$=0.001$; the dielectric constant $\epsilon=16$, smaller than that of most of the perovskites; the coefficients of thermal expansion (CTE) $k_{\mathbf{a}}=5.1\times10^{-6}$ °C^{-1}, $k_{\mathbf{b}}=4.2\times10^{-6}$ °C^{-1}, $k_{\mathbf{c}}=11.7\times10^{-6}$ °C^{-1}, which differ slightly from that found for YBCO ($k_{\mathbf{a}}=14\times10^{-6}$ °C^{-1}, $k_{\mathbf{b}}=12\times10^{-6}$ °C^{-1}, $k_{\mathbf{c}}=25\times10^{-6}$ °C^{-1}).

A brief description of the processing technique is as follows: KrF excimer laser (Lambda Physik LPX 305icc: $\lambda=248$ nm, pulse duration of 25 ns, max. output of 850 mJ/pulse) was used to ablate stoichiometric ceramic targets of $YBa_2Cu_3O_{7-x}$ and $PbZr_{0.52}Ti_{0.48}O_3$. The YBCO layer is grown at a substrate temperature of 710 °C in a 200 mTorr oxygen partial pressure ambient, at a laser beam fluence of 2 J/cm^2 and pulse repetition rate of 10 Hz. At this condition the deposition rate was found to be around 16.7 nm/min. The

[a]Also at the Dept. of Condensed Matter Physics, Royal Institute of Technology, S-100 44 Stockholm, Sweden. Electronic mail: grishin@kth.se

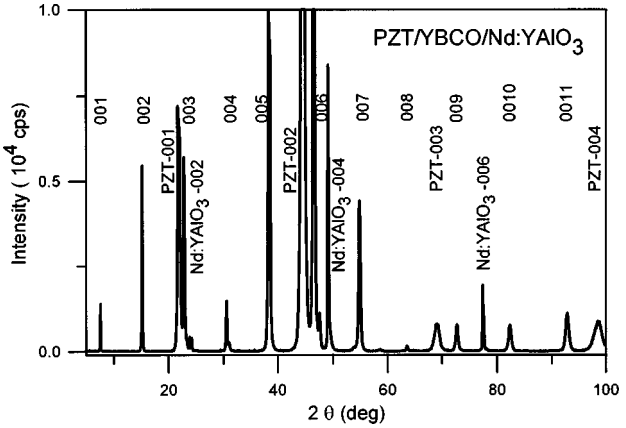

FIG. 1. θ-2-θ XRD scan of the PZT(400 nm)/YBCO(200 nm)/Nd:$YAlO_3$ structure. (00l) indices define the reflections from YBCO.

deposition is followed by an anneal at 450 °C in 600 Torr oxygen for 60 min. After this, deposition of the PZT layer is done at a substrate temperature of 550 °C in a 100 mTorr oxygen pressure, the same laser energy density and repetition rate lowered to 5 Hz, which result in the PZT deposition rate of 26.7 nm/min. Finally the whole heterostructure is annealed in an oxygen pressure of 600 Torr at 400 °C for 60 min and then cooled down to room temperature. To make capacitive cells for electrical characterization circular electrodes with a diameter of 200 μm have been prepared *ex situ* by thermally evaporation of gold through the contact mask onto the front PZT surface at room temperature.

Figure 1 shows the θ–2θ x-ray diffraction pattern (Cu $K\alpha$ radiation) of the PZT/YBCO/Nd:$YAlO_3$ heterostructure. The XRD spectrum consists of only the narrow (00l) PZT, YBCO, and Nd:$YAlO_3$ diffraction peaks. The observed high degree of c-axis orientation in both PZT and YBCO layers is also suggested by the rocking curves presented in Fig. 2. Their full widths at half-maximum (FWHM) are 1.15°, 0.48°, and 0.28° for PZT-002, YBCO-006, and Nd:$YAlO_3$-004 neighboring reflections, respectively. The calculated lattice parameters of PZT (a was found to be 0.397 nm while $c/a=1.029$) and YBCO ($b=0.385$ nm, $c/b=3.0469$) indicate the perfect crystalline film-film as well as films-Nd:$YAlO_3$ (pseudocubic $a_{pc}=b_{pc}=0.3715$ nm) matching. Fabricated heterostructures have been found highly oriented in the (**a**,**b**) plane. It is clearly seen from the fourfold symmetry φ scan of the PZT-113, YBCO-0110, and Nd:$YAlO_3$-116 reflections shown in Fig. 3. Summarizing XRD information we arrive at the conclusion that the epitaxial relationship of the PZT/YBCO bilayer on Nd:$YAlO_3$ is

$$(001)\mathrm{PbTiO_3}\|(001)\mathrm{YBa_2Cu_3O_{7-x}}\|(001)\mathrm{Nd{:}YAlO_3},$$

$$[100]\mathrm{PbTiO_3}\|[100]\mathrm{YBa_2Cu_3O_{7-x}}\|[110]\mathrm{Nd{:}YAlO_3}. \quad (1)$$

High dielectric constant $\epsilon=950$ and relatively low loss tan $\delta=0.04$, which are almost frequency independent in the range 100 Hz–100 kHz; high electric resistivity ρ (150 kV/cm) $=6\times10^{11}\Omega$ cm of the PZT film and no visible fatigue after 10^7 short bipolar pulses switching indicate excellent electrical performance of fabricated heterostructures. Typical $P-E$ hysteresis loop, measured by a Sawyer–Tower circuit at frequency of 1 kHz, is shown in Fig. 4 by circular symbols. The pulsed testing setup RT66A (Radiant Technologies) operating in the ''fast mode'' gives almost the same $P-E$ trace. Remnant polarization P_r and the coercive field E_c were found to be 32 μC/cm^2 and 35 kV/cm.

Crystalline misalignment and *finite grain size* are two important issues which control the characteristics of polarization loop in ferroelectrics. To clarify such a correlation between film electrical performance and crystal structure we used the Landau mean-field theory. The Gibbs potential for an uniaxial ferroelectric presented in the form[9]

$$G=G_0+\frac{a}{2}(T-T_c)P^2+\frac{b}{4}P^4-\mathbf{E}\cdot\mathbf{P}. \quad (2)$$

Here, T_c is the Curie temperature, constants a, $b>0$, **P** and **E** are the polarization and electric field vectors. At temperatures below T_c the equilibrium value of the polarization, found as the minimum of the potential G, is given by

$$\frac{E}{E_c}=\frac{3^{3/2}}{2}\cdot\left[\left(\frac{P}{P_r}\right)^3-\frac{P}{P_r}\right],$$
$$E_c\equiv\frac{2\cdot a^{3/2}\cdot(T_c-T)^{3/2}}{3^{3/2}\cdot b^{1/2}},\quad P_r\equiv\left(\frac{a}{b}\right)^{1/2}(T_c-T)^{1/2}. \quad (3)$$

E/E_c vs P/P_r curve, plotted by solid line A in Fig. 4, describes the hysteresis of a polarization in an infinite ideal

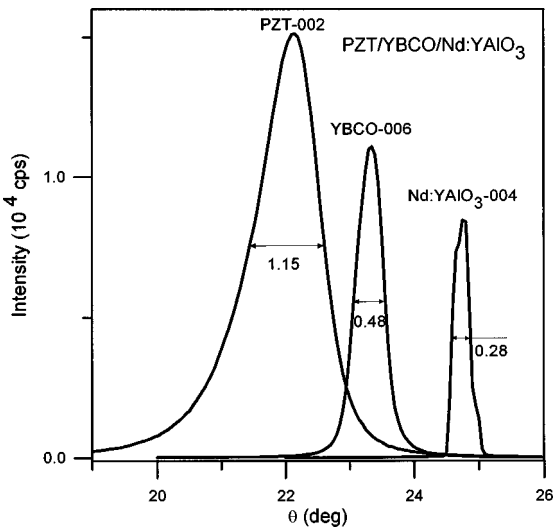

FIG. 2. XRD rocking curves (ω scans) of neighboring PZT-002, YBCO-006, and Nd:$YAlO_3$-004 reflections.

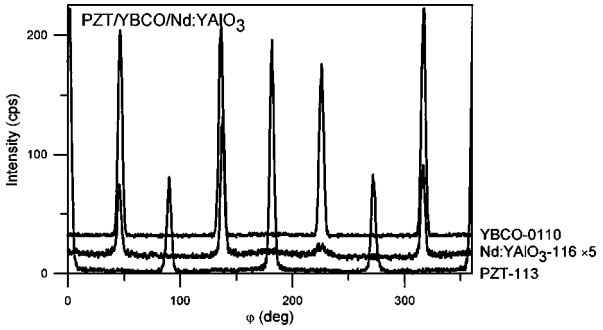

FIG. 3. φ scans of reflections from the YBCO-0110, Nd:$YAlO_3$-116 (multiplied by a factor of 5) and PZT-113 crystallographic planes measured at oblique geometry: the detector position $2\theta_{det}=86.79°$, 81.02°, 77.83°, the sample position $\theta_{sam}=60.39°$, 58.75°, and 64.35° correspondingly.

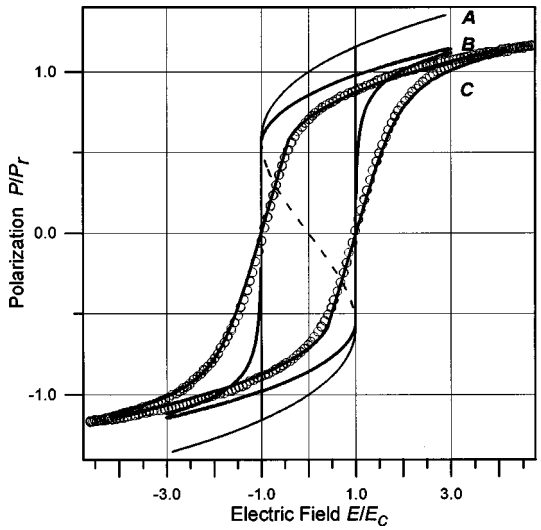

FIG. 4. Ferroelectric hysteresis loops. The polarization and electric field are normalized to the nominal values of the remanant polarization P_r and the coercive field E_c given by Eq. (3). Line **A** is the theoretical square polarization loop in an infinite uniaxial ferroelectric. The dashed part of line **A** shows the branch with the negative differential polarizability; **B** is the theoretical curve which accounts for only ferroelectric crystallite misalignment with FWHM parameters of $2\Omega=1.15°$ taken from the experimental rocking curve PZT-002 in Fig. 2. **C** is the theoretical curve accounting both the accidential misalignment ($2\Omega=1.15°$) and the shape of crystallites which were found to be *prolate ellipsoids* with the length-to-diameter ratio of 140. Symbol (o) shows experimental hysteresis loop in Au/PZT(400 nm)/YBCO(200 nm)/Nd:$YAlO_3$ capacitor structure measured by Sawyer–Tower circuit at a frequency of 1 kHz, $P_r=32\ \mu C/cm^2$, $E_c=35$ kV/cm.

single crystal. At a strong electric field $|E|/E_c>1$ the polarization changes reversibly and increases as $P/P_r=(2E/3^{3/2}E_c)^{1/3}$ with the field increase. When the electric field decreases, the abrupt irreversible switching of polarization $\Delta P=\sqrt{3}\cdot P_r$, occurs at the coercive field $|E|=E_c$.

To account for random ferroelectric crystallite orientation we introduce the polar c-axis distribution function $f(\omega)$ and express the averaged value of the normal component of polarization $\langle P(E)\rangle$ through the integral

$$\langle P(E)\rangle=\int_0^{\pi/2} d\omega\cdot\sin\,\omega\cdot f(\omega)\cdot P(E\,\cos\,\omega)\cdot\cos\,\omega. \tag{4}$$

Here, a given crystallite orientation is defined by the angle ω between actual polar axis and the normal to the film. Such accidental crystallite orientational variations results in the reduction of the effective electric field and the remnant polarization both proportional to $\cos\,\omega$. To approximate real c-axis angular distribution, represented by the rocking curve PZT-002 in Fig. 2, the normalized Lorentzian function

$$f(\omega)=\frac{\sqrt{1+\sin^2\,\Omega}}{\ln(\sqrt{1+\sin^2\,\Omega}+1/\sin\,\Omega)\cdot(\sin^2\,\Omega+\sin^2\,\omega)},$$
$$\int_0^{\pi/2} d\omega\cdot\sin\,\omega\cdot f(\omega)=1 \tag{5}$$

has been used. Here, the angle 2Ω gives the full width at half-maximum (FWHM) of the rocking curve in the ω scan (Fig. 2, so-called mosaic broadening). The calculated $\langle P(E)\rangle$ dependence with the FWHM PZT-002 parameter $2\Omega=1.15°$ is shown in Fig. 4 by solid line **B**. The remnant polarization decreases, the $P-E$ loop is smoothed and abrupt polarization switching disappears because different crystallite switching occurs at different fields $E=E_c/\cos\,\omega$.

To compare theoretical prediction with the experimental data the depolarizing electric fields must also be considered. Assuming crystallites to be ellipsoidal we can express the macroscopic electric field inside the ellipsoid $\mathbf{E}^{(i)}$ through the external electric field $\mathbf{E}^{(e)}$, polarization $\mathbf{P}$ and the tensor of depolarizing coefficients $\hat{N}$: $\mathbf{E}^{(i)}=\mathbf{E}^{(e)}-4\pi\hat{N}\mathbf{P}$. To account for the depolarizing field the theoretical curve **B** in Fig. 4 and the expression (4) should be considered as the constitutive relationship between the polarization $\langle P\rangle$ and the internal electric field $E^{(i)}$. Then the final theoretical dependence $\langle P\rangle$ versus $E^{(e)}$, accounting both crystal structure imperfections and depolarizing effects, can be easily obtained by replotting the polarization loop in coordinates $\langle P\rangle$ vs $E^{(i)}+4\pi N\langle P\rangle$. This dependence is shown in Fig. 4 by solid line **C**. It gives a fairly good fit with the experimental data if the depolarizing coefficient is chosen to be $N=2.37\times10^{-4}$. Since the coefficient N determines the maximum value of the differential polarizability: $[dP/dE^{(e)}]_{\max}=1/4\pi N$, it can also be determined directly from the maximum slope of the experimental $P-E^{(e)}$ loop. The small value of the obtained depolarizing coefficient corresponds to the prolate ellipsoid in the longitudinal electric field with the dimensional (length/diameter) ratio of 140. This conclusion coincides with the electron microscope observations on the column growth of highly c-axis oriented ferroelectric films.[5,10]

In conclusion, the epitaxial $PbZr_{0.52}Ti_{0.48}O_3/YBa_2Cu_3O_{7-x}$ thin film heterostructures have been grown *in situ* onto the Nd:$YAlO_3$ single-crystal substrate using the KrF PLD technique. High long term endurance, relatively high remnant polarization, and dielectric constant with low loss indicate excellent ferroelectric performance. The theory of the hysteresis loop shape has been developed to account for a slight crystallite polar axis misalignment and the depolarizing effect in epitaxial ferroelectric films. The only fitting parameter depolarizing coefficient N was found to be 2.37×10^{-4} which corresponds to *prolate ellipsoidal* shaped crystallites with the length-to-diameter ratio of 140.

The authors wish to thank Dr. I. M. Syvorotka from the Research Production Amalgamation ''Carat'' (L'viv, Ukraine) for providing them with Nd:$YAlO_3$ substrates.

[1] J. F. Scott and C. A. Araujo, Science **246**, 1400 (1989).
[2] D. J. Taylor, P. K. Larsen, and R. Cuppens, Appl. Phys. Lett. **64**, 1392 (1994).
[3] O. Auciello, M. A. Ray, D. Palmer, J. Duarte, G. E. McGuire, and D. Temple, Appl. Phys. Lett. **66**, 2183 (1995).
[4] G. J. M. Dormans and P. K. Larsen, Appl. Phys. Lett. **65**, 3326 (1994).
[5] *Pulsed Laser Deposition of Thin Films*, edited by D. B. Chrisey and G. K. Hubler (Wiley, New York, 1994).
[6] O. Auciello and R. Ramesh, Mater. Res. Bull. **21**, 31 (1996).
[7] I. Tsukada and K. Uchinokura, Jpn. J. Appl. Phys., Part 2 **30**, L1468 (1991); J. Appl. Phys. **78**, 364 (1995).
[8] A. M. Grishin, G. V. Gusakov, A. B. Mukhin, N. Yu. Starostyuk, D. I. Savitskii, and I. M. Syvorotka, JETP Lett. **57**, 519 (1993).
[9] L. D. Landau and E. M. Lifshitz, *Electrodynamics of Continuous Media, Course of Theoretical Physics* (Addison–Wesley, Reading, MA, 1960), Vol. 8.
[10] R. E. Leuchtner, K. S. Grabowski, D. B. Chrisey, and J. S. Horowitz, Appl. Phys. Lett. **60**, 1193 (1992).